THE ASTROPHYSICAL JOURNAL, 458:580–599, 1996 February 20

IUE OBSERVATIONS OF YOUNG CLUSTERS IN THE LARGE MAGELLANIC CLOUD

ERIC M. WILCOTS[1,2]
National Radio Astronomy Observatory, P.O. Box O, Socorro, NM 87801
PAUL W. HODGE
University of Washington, Department of Astronomy, FM-20, Seattle, WA 98195
AND
NICHOLE KING
New Mexico State University, Astronomy Department, Box 30001/Department 4500, Las Cruces, NM 88003-8001
Received 1994 November 17; accepted 1995 August 25

ABSTRACT

We present the results of a study of the ultraviolet properties of the most massive stars in two young clusters in the Large Magellanic Cloud (LMC), NGC 1770 and NGC 2014. Although there is some variation across each cluster, we find that the properties of the interstellar extinction toward these clusters are consistent with those previously derived for stars in the Doradus Nebula region of the LMC. Using the *IUE* spectra and Kurucz model atmospheres, we have derived H-R diagrams for both clusters and find that: (1) there appear to have been two episodes of massive star formation in NGC 1770, one 4–5 $\times$ 10^6 yr ago and the other $\sim$10 $\times$ 10^6 yr ago; and (2) star formation in NGC 2014 appears to have been relatively coeval (2–5) $\times$ 10^6 yr ago. Our analysis of the properties of the winds of these stars supports earlier conclusions that although the terminal velocities of the stellar winds of these stars scale with the metallicity of the LMC, the mass loss rates do not.

Subject headings: Magellanic Clouds — open clusters and associations: individual (NGC 1770, NGC 2014) — stars: early-type — stars: mass loss — ultraviolet: stars

1. INTRODUCTION

The Large Magellanic Cloud (LMC) has proven to be a rich source of information about the properties of massive young stars, and the clusters and associations in which they reside. The studies conducted by Massey et al. (1989) and Parker (1993), for example, have done much to increase our understanding of the massive stellar population of LMC associations. Massey et al. (1995a) have recently surveyed the field stars in the LMC, and they find a large number of field O and B stars with similar statistical properties to those found in associations. While these studies have been largely optical, others have shown the usefulness of using ultraviolet spectroscopy to probe the physical properties of such young massive stars. Although this is a time-consuming approach, it is a reliable method for determining stellar temperatures, and the ultraviolet spectra provide an unambiguous determination of which stars are main-sequence stars and which are evolved giants (e.g., Conti, Garmany, & Massey 1986). In particular, the ultraviolet stellar lines of C IV and Si IV are diagnostics of the luminosity class of an O star (Walborn & Panek 1984) and probes of the stellar winds associated with these stars (e.g., Garmany & Conti 1985). The combination of these factors makes the ultraviolet study of the massive stars in clusters an excellent probe of the age and age spreads of these systems. Additionally, such studies also allow for an investigation of the properties of interstellar reddening (e.g., Murray-Hanson & Clayton 1993).

With this background we have conducted a study of the ultraviolet properties of a sample of young clusters in the LMC to determine the ages and age spreads of these clusters and the properties of the massive stars themselves. The LMC contains a wealth of massive star clusters of all ages (cf. van den Bergh 1991). While many of the brightest clusters have been studied using the *IUE* satellite (e.g., Cassatella, Barbero, & Geyer 1987), the youngest clusters have gone largely unstudied at ultraviolet wavelengths. This paper concentrates on the properties of two of the clusters selected for this study, NGC 1770 and NGC 2014. A third cluster, LH 72, is the subject of a second paper (Hodge et al. 1996).

NGC 1770 and NGC 2014 are particularly well suited to this program and its goals. They are both comprised of well-separated, luminous stars that have been optically identified as O or B spectral types. Additionally, both clusters are involved in large-scale H II regions. NGC 2014 is on the edge of the large Shapley III Constellation in the northeastern part of the LMC. It is one of several large H II regions (DEM 229) in a ring of current star formation activity. DeGioia-Eastwood, Meyers, & Jones (1993) have used optical photometry to determine that star formation in NGC 2014 has been coeval and was probably initiated by the expanding superbubble that makes up the Shapley III constellation. NGC 1770 sits in the H II region DEM 39, located at the western end of the bar. Note that the cluster SL 134 is embedded within the nominal confines of NGC 1770 (Lucke 1972). Both DEM 39 and DEM 299 are among the most luminous H II regions in the LMC (Kennicutt & Hodge 1986).

Table 1 lists the observed clusters and their various identifications. Our targets within each cluster were selected as those objects that have been identified as either O and B stars—many of the stars we have chosen have been classified by Sanduleak (1969), Conti et al. (1986), Fitzpatrick (1988), or Massey et al. (1995a)—and objects that appear to be bright and blue. A

[1] Jansky Fellow.
[2] Present address: Department of Astronomy, 475 N. Charter Street, University of Wisconsin, Madison, WI 53706.

TABLE 1

OBSERVED CLUSTERS

LH.....	12	76
Henize.....	91	57
DEM.....	39	229
NGC.....	1770	2014
IC.....	2117	...

list of the targeted stars and their optical identifications is given in Table 2. We list the spectroscopically based classification and the available photometry (gathered from several sources) for each star.

This paper is organized as follows: In § 2 we detail our observations and initial reductions. At the initial stage in the analysis of this data, we investigated the properties of the interstellar extinction toward each of these clusters. This is discussed in § 3. Given an understanding of the interstellar extinction, we then compared the observed spectra with the most recent (1992) versions of the Kurucz (1979) model stellar atmospheres to determine the best fit. This fitting procedure and the resulting H-R diagrams (HRDs) are presented and discussed in § 4. Finally, we discuss properties of the stellar winds associated with these stars in § 5.

2. OBSERVATIONS AND REDUCTIONS

We obtained low-resolution short-wavelength (1150 Å $\leq \lambda \leq$ 2000 Å) and long-wavelength (1900 Å $\leq \lambda \leq$ 3100 Å) spectra using the *IUE* satellite (Boggess et al. 1978). A detailed listing of the observations is given in Table 3, which provides information on the *IUE* catalog number, date of observation, exposure time, exposure level, and some comments. A handful of the spectra were somewhat underexposed, and they are listed here only for completeness. In addition to the objects specifically observed for this project, we retrieved the spectra for L2 and L17 (both in NGC 1770) from the *IUE* archives. The observational parameters for those spectra are also listed in Table 3.

The spectra were each calibrated using the *iuespec* program as prescribed by the *IUE* Regional Data Analysis Facility's manual. Once calibrated, the spectra were trimmed: the SWP spectra to 1151.0 Å $\leq \lambda \leq$ 1981.6 Å and the LWP spectra to 1981.6 Å $\leq \lambda \leq$ 3198.6 Å. Finally, the short- and long-wavelength spectra were merged, resulting in a single spectrum covering 1151.0–3198.6 Å. The last step of the reduction was to correct for the Galactic foreground extinction using the Seaton (1979) extinction law and an $E(B-V)$ of 0.019 (McNamara & Feltz 1980). The calibrated trimmed, and dereddened spectra are shown in Figure 1 for NGC 2014 and Figure 2 for NGC 1770.

3. INTERSTELLAR EXTINCTION

Since the ultimate goal of this study is the derivation of an HRD for each of the clusters, it is essential that we first understand the characteristics and magnitude of the interstellar

TABLE 2

OBSERVED STARS

Star (1)	Sk (2)	HDE (3)	Spectral Type (4)	V (5)	$(B-V)$ (6)	Reference (7)
			NGC 1770			
L2	−6811	...	...	12.4	−0.06	
L3	−6814	...	B2Iab	11.21	0.06	3
L16.....	...	...	...	13.19	0.00	
L17.....	−6815	32402	...	12.6	−0.25	
L22.....	...	...	...	14.22	−0.16	
L25.....	...	...	...	13.88	−0.17	
L26.....	−6812	258798	...	11.43	0.06	
L27.....	...	...	...	14.69	−0.38	
L30.....	...	...	...	13.67	−0.19	
L33.....	...	...	...	14.20	−0.19	
L34.....	...	...	...	13.85	−0.18	
L43.....	−6816	...	O7III	12.86	0.07	3
			NGC 2014			
L1	−67166	269698	O4If	12.27	−0.22	2
				12.31	−0.25	1
L21.....	−67167	...	O4If	12.54	−0.19	2
				12.59	−0.23	1
L51.....	−67173	...	B0Ia	11.80	−0.19	1, 5
				12.04	−0.12	4
L59.....	−67178b	...	B2Iab	12.21	−0.14	3
				12.31	−0.21	4
				12.13	−0.16	1
L70.....	−67159	...	...	12.83	−0.05	1
S4	−67174	269714	O9II	11.67	−0.18	2
			O8V	11.96	−0.19	4, 5
S6	−67176	269717	O8II	11.82	−0.16	3
			O7Ib			2
				11.91	−0.22	4

NOTES.—All photometry for stars in NGC 1770 was taken from Lucke 1972.

REFERENCES.—(1) Lucke 1972, (2) Fitzpatrick 1988, (3) Conti et al. 1986, (4) Degioia-Eastwood et al. 1993, (5) Massey et al. (1995a).

TABLE 3

OBSERVED STARS

Star	*IUE* Number	U.T. Date	Exposure (minutes)	Exposure (DN)	Comments
		NGC 1770			
L2	SWP 25899	1985 May 9	24.0	...	Archive
	LWP 05945	1985 May 9	24.0	...	Archive
L3	SWP 46394	1992 Dec 2	17.0	126	
	LWP 24413	1992 Dec 5	6.0	180	
L16.....	SWP 46396	1992 Dec 3	45.0	175	
	LWP 24412	1992 Dec 4	25.0	100	Underexposed
L17.....	SWP 14162	1981 Jun 3	8.0	...	Archive
	LWR 10767	1981 Jun 3	17.0	...	Archive
L22.....	SWP 46412	1992 Dec 5	60.0	160	
	LWP 24411	1992 Dec 4	50.0	190	
L25.....	SWP 45307	1992 Aug 9	40.0	220	
	LWP 24395	1992 Dec 3	45.0	250	
L26.....	SWP 45306	1992 Aug 9	25.0	203	
	LWP 24414	1992 Dec 5	6.0	184	
L27.....	SWP 46414	1992 Dec 5	20.0	40	Underexposed
	LWP 23665	1992 Aug 8	40.0	100	Underexposed
L30.....	SWP 46395	1992 Dec 3	40.0	130	
	LWP 23668	1992 Aug 9	40.0	250	
L33.....	SWP 46397	1992 Dec 3	50.0	40	Underexposed
L34.....	SWP 46413	1992 Dec 5	50.0	210	
	LWP 24397	1992 Dec 3	30.0	135	Underexposed
L43.....	LWP 23667	1992 Aug 9	20.0	150	Underexposed
		NGC 2014			
L1	SWP 43352	1991 Dec 9	10.0	235	
	LWP 21982	1991 Dec 10	5.0	180	
L21.....	SWP 43354	1991 Dec 10	10.0	210	
	LWP 21984	1991 Dec 10	6.0	179	
L51.....	SWP 43357	1991 Dec 10	10.0	185	
	LWP 21989	1991 Dec 11	5.0	174	
L59.....	SWP 43356	1991 Dec 10	10.0	155	
	LWP 21986	1991 Dec 10	6.0	170	
L70.....	SWP 43353	1991 Dec 10	15.0	200	
	LWP 21983	1991 Dec 10	7.0	160	
S3	SWP 40215	1990 Nov 28	5.0	117	
	LWP 19296	1990 Nov 28	5.0	163	
S4	SWP 40213	1990 Nov 28	3.0	106	
	LWP 19294	1990 Nov 27	3.0	134	
S6	SWP 40216	1990 Nov 28	7.0	220	
	LWP 19297	1990 Nov 28	5.0	213	

reddening toward these clusters. We accounted for Galactic foreground extinction in the reduction stage of this project; here, we detail our approach to handling the interstellar reddening within each cluster. The properties of the interstellar extinction curve in the LMC have been well studied, notably in the work of Nandy et al. (1981, hereafter referred to as N81) and Fitzpatrick (1985 1986, hereafter referred to as F85 and F86, respectively). There is ample evidence that the properties of the interstellar extinction curve vary with position across the LMC (F85; F86; Clayton & Martin 1985). Specifically, there is a distinct difference between the extinction curves inside and outside of the 30 Dor region (F85; F86). The 30 Dor extinction curves (e.g., N81; F85) tend to have weaker 2175 Å bumps and steeper rises toward the far-UV than their counterparts outside of 30 Dor. In addition to this variation across the LMC, recent photometric studies of several OB associations in the LMC indicate that the amount of reddening may vary within a particular cluster (e.g., Parker 1993). Similarly, Wilcots (1994) found that the amount of reddening may vary within a given H II region.

The data we collected for this study allowed us to investigate the properties of the interstellar extinction in these clusters. In column (4) of Table 2 we have listed the spectral type for several stars as derived from optical spectroscopic work. Using the calibrations of Garmany & Fitzpatrick (1988) for O stars and Humphreys & McElroy (1984) for B stars, we obtained $T_{\rm eff}$ and the bolometric correction (BC) for each classified star. With this information we determined which Kurucz stellar atmosphere model(s) best match the observed spectral type. This step amounted to a selection of the most appropriate combination of $T_{\rm eff}$ and BC from the library of Kurucz models. We then scaled the model atmosphere by the angular diameter, θ^2, of the star in question. This is defined as: $\theta^2 = F_V(\text{model})/F_V(\text{observed})$, where $F_V(\text{model})$ is the surface flux at V listed in the models and $F_V(\text{observed})$ is the observed flux at V. Once the spectra were properly scaled, the ratio of the observed spectrum to that of the model gave a direct estimate of the amount of interstellar extinction as a function of wavelength, A_λ. While this is an interesting number in and of itself, we are more interested in seeing how the extinction in

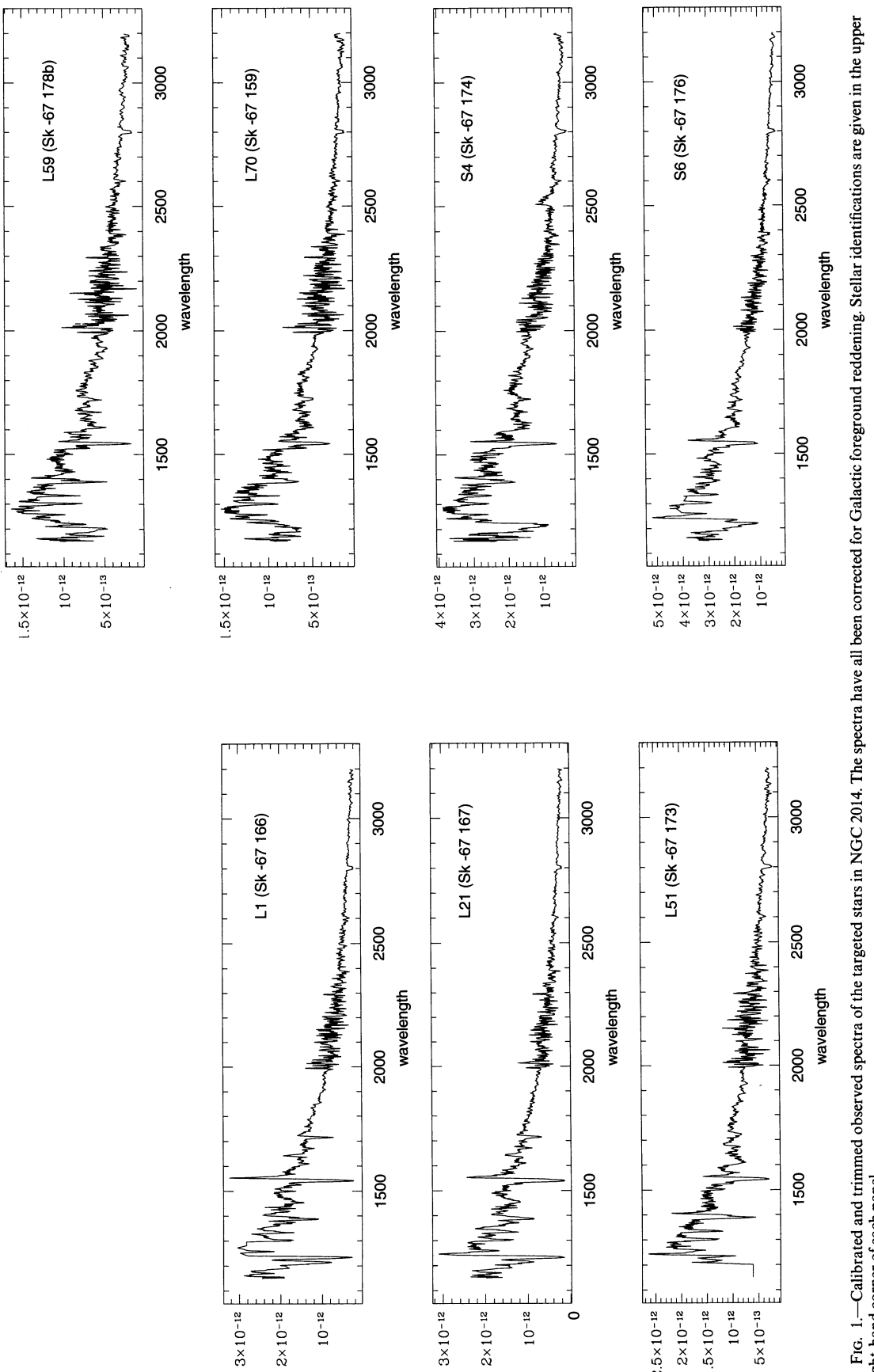

FIG. 1.—Calibrated and trimmed observed spectra of the targeted stars in NGC 2014. The spectra have all been corrected for Galactic foreground reddening. Stellar identifications are given in the upper right-hand corner of each panel.

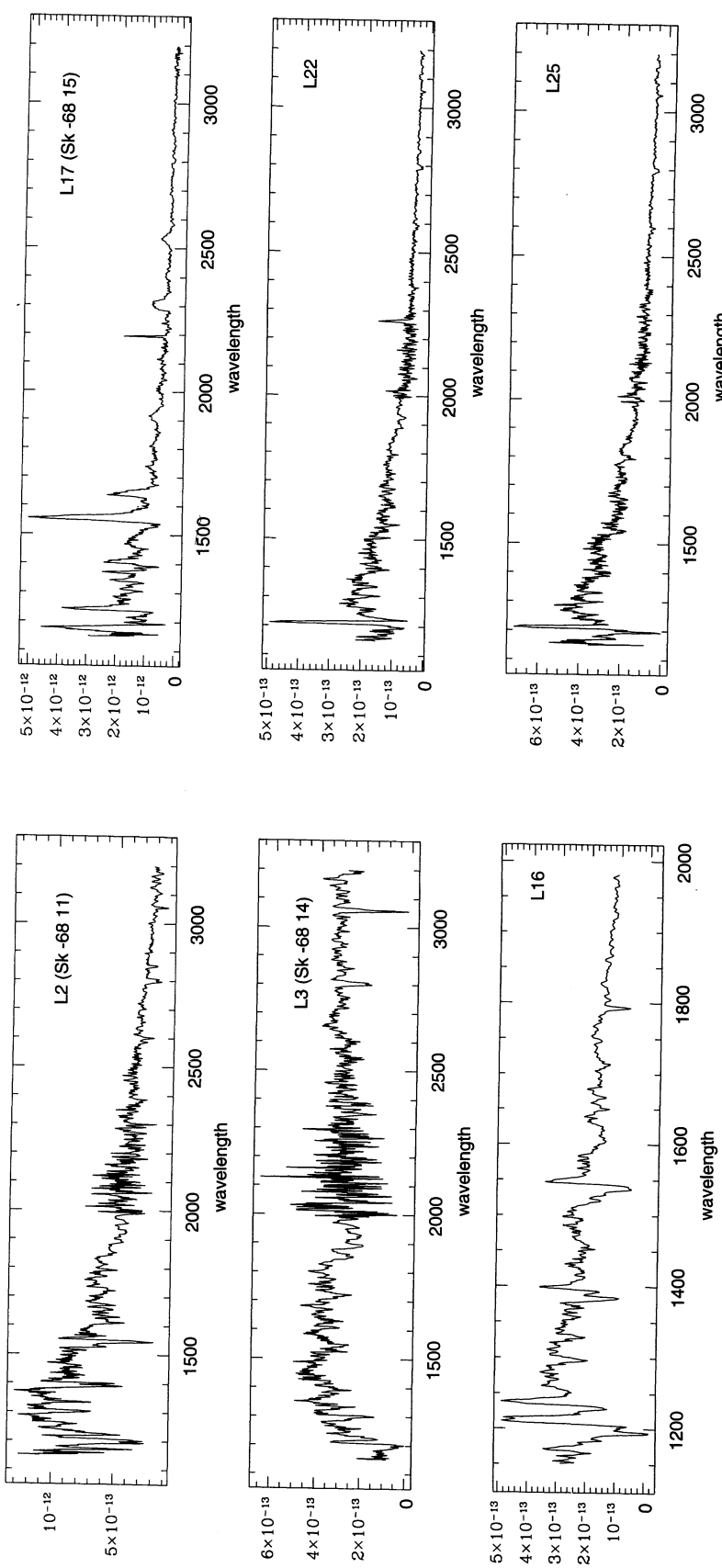

FIG. 2.—Same as Fig. 1, but for the targeted stars in NGC 1770

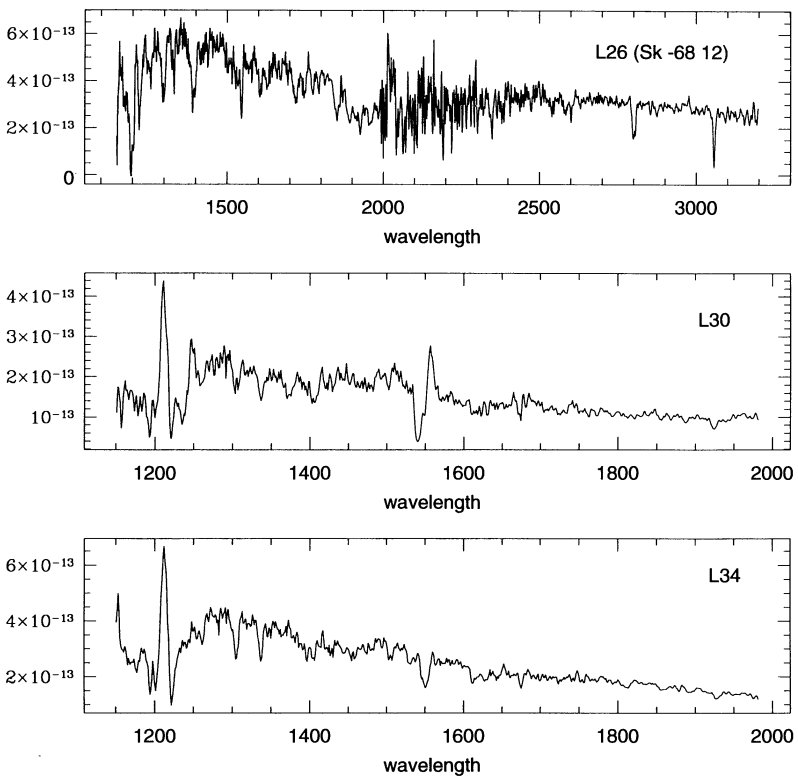

FIG. 2—*Continued*

these particular clusters compares with extinction curves derived in other parts of the LMC. Typically, extinction curves are presented as $E(\lambda - V)/E(B - V)$ and are normalized such that $A_V = 0$ and $E(B - V) = 1.0$. By simply scaling the model spectra by the angular diameter, we have effectively normalized the extinction curve to $A_V = 0$. We estimated the observed reddening from the difference between the observed values of $(B - V)$ taken from the literature (see Table 2) and the values of $(B - V)$ for the models. Normalizing this, such that $E(B - V) = 1.0$, we derived an extinction curve directly comparable to those in the literature.

The results of this exercise are presented in Figures 3–7, where we have plotted our extinction curve (*filled squares*), as well as those of N81 (*open squares*) and F86 (*open circles*). Note that the N81 curve is essentially identical to the 30 Dor curve derived by F85. We fitted a continuum to each of the observed spectra, then the fitted continua and the model spectra were binned into 50 Å bins. The extinction curves were derived from these binned spectra using the technique described in the previous paragraph. Printed in the upper right-hand corner of each panel are the star's name, the observed V magnitude and $(B - V)$ colors, and our estimate of the reddening. We typically compared the observed spectra with several model spectra to provide us with a sense of how the derived curves were affected by small changes in the models. One can see from the figures that these effects are almost negligible. We list each model and its basic parameters in Table 4.

The first two stars, L1 and L21, have been spectroscopically classified by Fitzpatrick (1988) as O4If stars. In Figures 3*a* and *b* we show the curves for L1 using both Fitzpatrick's (1988) and Lucke's (1972) photometry. In both cases, we have derived a curve for each of the three models listed in Table 4. It is clear

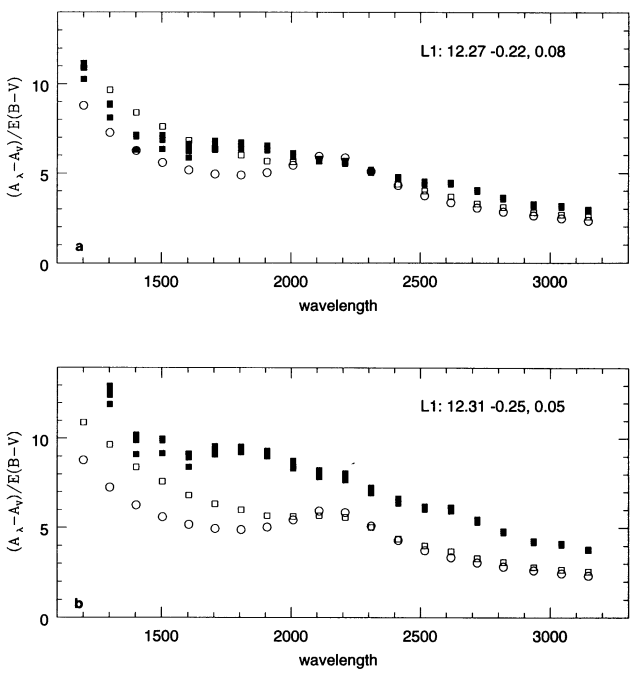

FIG. 3.—Comparison of reddening curves for L1. The curve we have derived from the comparison of the known spectral type and the Kurucz model atmospheres is shown by the filled squares. The curves of N81 and F86 are shown as open squares and open circles, respectively. The optical photometry $(V, B - V)$ used to derive the extinction curves is given in the upper right-hand corner of each panel. The last entry on the line is the derived value of $E(B - V)$.

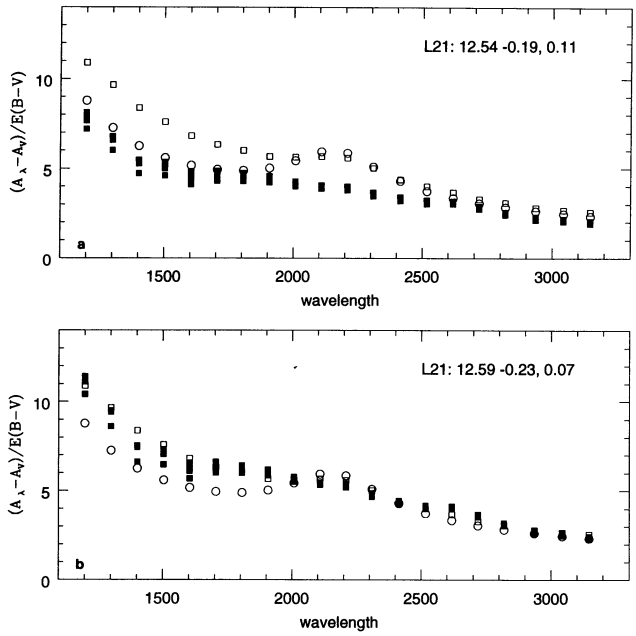

FIG. 4.—Same as Fig. 3, but for L21

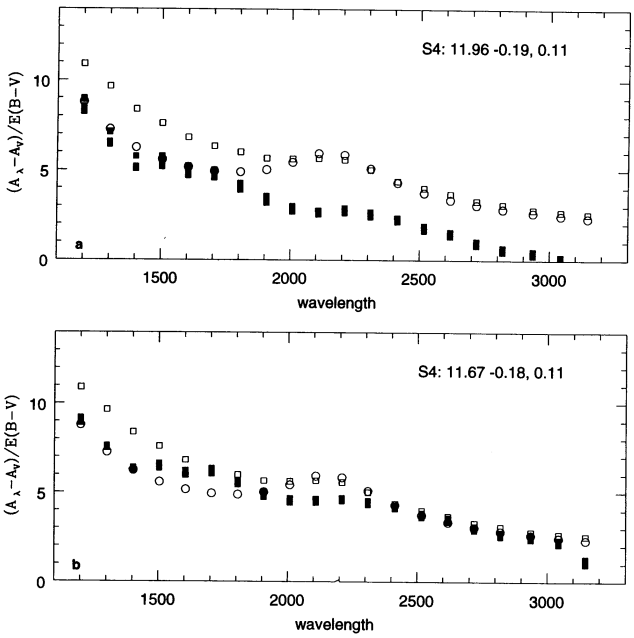

FIG. 6.—Same as Fig. 3, but for S4

that the combination of the spectral type and the photometry of Lucke (1972) does not yield a physically meaningful extinction curve. In Figure 3*a* we see that the derived curve using the photometry of Fitzpatrick (1988) is quite similar to the N81 curve: there is a lack of a strong 2175 Å feature, as well as a steep rise in the far-UV. The Lucke (1972) photometry leads to a "high" extinction curve that is consistently offset above either the N81 or the F85 curve. Given that there is near uniformity in extinction curves in many different environments longward of the 2175 Å bump (Calzetti, Kinney, & Storchi-Bergmann 1994), we feel that this offset reflects errors in the photometry. The situation is similar for L21, but with the roles reversed. Using Lucke's photometry (Fig. 4*a*), we derive an extinction curve that is quite similar to the N81 curve. Fitzpatrick's (1988) photometry yields a somewhat shallower curve (Fig. 4*b*), although it also lacks the 2175 Å feature.

The combination of the published photometry (Lucke 1972; Conti et al. 1986) and the derived spectral type of B0 Ia for L51 (Conti et al. 1986) yields the extinction curves shown in Figures 5*a* and 5*b*. Clearly, neither of these combinations works particularly well. In Figure 5*c* we show the results of simply taking the average values of V and $(B - V)$. We again derive an

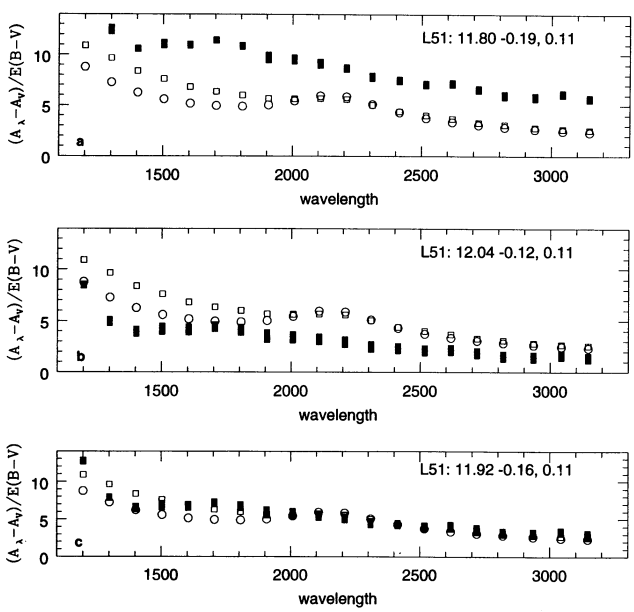

FIG. 5.—Same as Fig. 3, but for L51

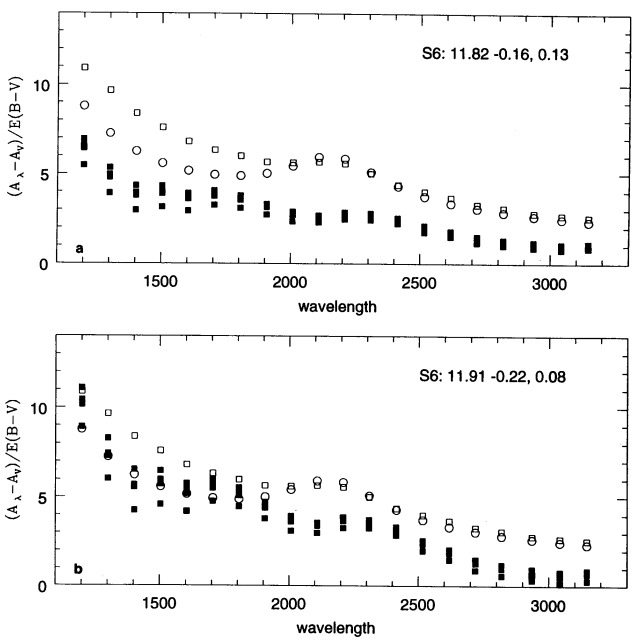

FIG. 7.—Same as Fig. 3, but for S6

TABLE 4

PARAMETERS FOR FITTING EXTINCTION CURVES

STAR	MODEL 1				MODEL 2				MODEL 3			
	V	$(B-V)$	$T_{\rm eff}$	log g	V	$(B-V)$	$T_{\rm eff}$	log g	V	$(B-V)$	$T_{\rm eff}$	log g
NGC 2014												
L1 (O4 If)	12.27	−0.22	40,000	4.50	12.31	−0.25	40,000	4.50	...	...	...	...
			40,000	5.00			40,000	5.00				
			42,500	5.00			42,500	5.00				
			45,000	5.00			45,000	5.00				
L21 (O4 If)	12.54	−0.19	40,000	4.50	12.59	−0.23	40,000	4.50	...	...	...	...
			40,000	5.00			40,000	5.00				
			42,500	5.00			42,500	5.00				
			45,000	5.00			45,000	5.00				
L51 (B0Ia)	11.80	−0.19	27,000	3.50	12.04	−0.12	27,000	3.50	11.92	−0.16	27,000	3.50
			28,000	3.50			28,000	3.50			28,000	3.50
			29,000	3.50			29,000	3.50			29,000	3.50
L59 (B2 Iab)	12.21	−0.14	17,000	2.50	12.31	−0.21	17,000	2.50	12.24	−0.08	17,000	2.50
			18,000	2.50			18,000	2.50			18,000	2.50
			19,000	2.50			19,000	2.50			19,000	2.50
S4 (O9 II, O8 V)	11.96	−0.19	37,500	4.50	11.67	−0.18	37,500	4.50	...	...	...	...
			37,500	5.00			37,500	5.00				
			40,000	4.50			40,000	4.50				
			40,000	5.00			40,000	5.00				
S6 (O7 Ib, O8 II)	11.82	−0.16	35,000	4.00	11.91	−0.22	35,000	4.00	...	...	...	...
			35,000	4.50			35,000	4.50				
			35,000	5.00			35,000	5.00				
			37,500	4.50			37,500	4.50				
			37,500	5.00			37,500	5.00				
NGC 1770												
L3 (B2 Iab)	11.21	0.08	17,000	2.50								
			18,000	2.50								
			19,000	2.50								

extinction curve that is similar to the 30 Dor curves of N81 and F85. This is also true of the form of the curves in Figures 5*a* and 5*b*.

Fitzpatrick (1988) and Massey et al. (1995a) have derived similar spectra types for S4; these are O9II and O8V, respectively. Both Fitzpatrick (1988) and DeGioia-Eastwood et al. (1993) have published photometry on this star, and the resulting extinction curves are shown in Figures 6*a* and 6*b*. The Fitzpatrick (1988) photometry results in an intermediate extinction curve (Fig. 6*b*): the weakness of the 2175 Å bump is consistent with the 30 Dor curves, while the shallowness of the rise in the far-UV is consistent with the F86 curves. The combination of the DeGioia-Eastwood et al. (1993) photometry and the known spectral type (Fig. 6*a*) does not yield a reasonable extinction curve, although the shape of the curve is similar to that seen in Figure 6*a*.

In Figures 7*a* and 7*b* we show the derived extinction curves for S6 using the photometry of Fitzpatrick (1988) and DeGioia-Eastwood et al. (1993). Neither set of photometry seems to go with the observed spectral type of O7Ib (Fitzpatrick 1988) or O8II (Conti et al. 1986). If anything, the derived extinction curve appears to be steeper in the far-UV than either the N81 or the F86 curves. Again, the vertical offsets away from both the N81 and the F86 curves reflect uncertainties in the photometry.

We have not shown the derived curve for L59 (Sk-67 178b) for the reason that the combination of the published photometry (Lucke 1972; Conti et al. 1986; DeGioia-Eastwood et al. 1993) and the spectra type of B2Iab (Conti et al. 1986) yields an entirely unphysical result—in all cases, the observed, and presumably reddened spectrum, has a larger flux than the model spectrum.

What, if anything, can we learn from these extinction curves? Most importantly, problems with the photometry (e.g., the sometimes large differences between the published photometry for a given star) render this process highly uncertain. Uncertainties in $(B-V)$ and V act to scale the derived extinction curves vertically on the plots shown in Figures 3–7, while leaving the slopes relatively unchanged. The vertical offsets seen in many of the derived curves could be the result of uncertain photometry. Given that optical spectroscopy is an excellent means by which to derive the spectral types of O and B stars, it is not likely that the classifications are dramatically incorrect. It is also quite possible that the correlation between the observed spectral type, the calibration (Fitzpatrick & Garmany 1990), and the Kurucz model atmosphere is not a tight one. For example, Fitzpatrick & Garmany (1990) list a value for the $T_{\rm eff}$ and the BC for each type of star. There are very few cases in which there is a Kurucz model with those same values of $T_{\rm eff}$ and BC; in most cases, the model predicts a more negative BC for a given $T_{\rm eff}$. This is further compounded by the lack of low log g model atmospheres with high $T_{\rm eff}$.

Even with these uncertainties, we can glean some interesting information from the derived extinction curves. First, there is a consistent lack of strong 2175 Å features in these curves. Second, most of the curves rise more steeply in the far-UV than the non-30 Dor extinction curves would allow. Third, the derived reddenings appear to be rather modest and consistent with the global values for NGC 2014/DEM 229 derived by DeGioia-Eastwood et al. (1993) and Caplan & Deharveng

(1986). Based on these points, we conclude that the interstellar extinction toward NGC 2014 is best represented by a 30 Dor-like curve with a relatively modest amount of reddening.

NGC 1770 is not as rich in previously classified stars as is NGC 2014. We were further limited by the fact that we were only able to obtain an LWP spectrum of L43. Thus, our derivation of the extinction curve in NGC 1770 is restricted to L3. Following the same analysis detailed above, we derived the extinction curve plotted as solid squares in Figure 8. It appears that the extinction curve toward this star is quite comparable to the N81 curve; particularly, it has a weak 2175 Å bump and steep rise shortward of that. The implied reddening is nearly twice that of NGC 2014. Given these observations, we proceeded with the analysis of the stars in that cluster using the N81 extinction curve as well.

4. H-R DIAGRAMS

Aside from the reddening, the most critical parameter we need in order to assemble an HRD for each of these clusters is the $T_{\rm eff}$ of the stars in question. We have chosen to derive $T_{\rm eff}$ for each star by finding the model spectrum that best fits the observed data and using the $T_{\rm eff}$ of that model. For the stars in NGC 2014, each model spectrum was first "reddened" using the N81 extinction curve and $E(B-V)$ values of 0.06, 0.09, 0.12, and 0.15. We used the N81 curve and $E(B-V)$ values ranging from 0.06 to 0.27 in NGC 1770. The wider range of reddenings was necessary, because we have limited a priori knowledge of the amount of reddening toward NGC 1770. As a result, each observed spectrum was compared with a matrix of models of different reddenings and $T_{\rm eff}$. Additionally, for a given temperature there is a model for each of the several values of log g. In Figure 9 we demonstrate the range of models. In Figure 9*a* we show the five models with a $T_{\rm eff}$ of 28,000 K and gravities (log g) ranging from 3.0 to 5.0. One can see that these models are nearly indistinguishable from one another, especially longward of 1500 Å. Shortward of this, there is a significant difference between the lowest and the highest gravity models. Given the signal-to-noise ratio (S/N) of our spectra (Fig. 1–2), we were only able to distinguish between these extremes. We were also restricted by the lack of low log g models for the O stars. In Figure 9*b* we show the differences between models of different temperatures and a given log g. Each plotted spectrum is 1000 K hotter than the preceding (lower) one. From this we estimated that our spectra allowed us to determine the $T_{\rm eff}$ of a given star to within ± 1000 K. We show the dramatic effects of increasing the reddening in Figure 9*c*. We have reddened a single model spectrum ($T_{\rm eff}$ = 28,000, log g = 5.0) using an $E(B-V)$ of 0.06 (*top curve*), 0.09, 0.12, and 0.15 (*bottom curve*). The S/N of a spectra allowed us to distinguish between these steps in the reddening.

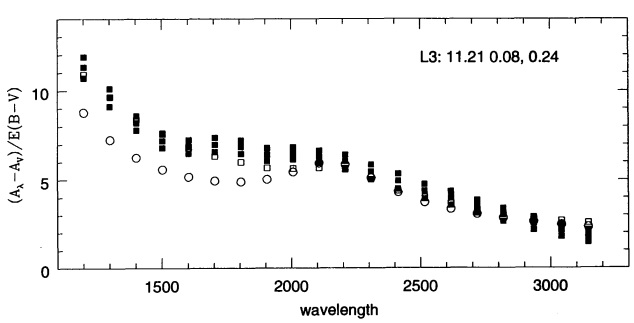

FIG. 8.—Same as Fig. 3, but for L3

Each model spectrum was scaled by θ^2, and we then compared each reddened and scaled model spectrum to the observed spectrum. We carried out a χ^2 analysis to determine the best fit from amongst all of the models. The results of our fitting procedure are shown in Figures 10 and 11, where we plot the observed spectrum for each star overlayed with the best-fitting model spectra. For the reasons detailed above, there were several model spectra that could be fitted to the data, and this is reflected in the figures. The parameters of each model are listed in Tables 5A and 5B. Those stars for which we had classifications were fitted with those models whose parameters were consistent with the spectral types. As can be seen in the figures, these spectra were well fitted by the appropriate Kurucz models. L70 was the only star in NGC 2014 for which we did not have a spectral classification, but it was also well fitted by a small range of Kurucz models. From these fits it appears that the reddening in NGC 2014 is a rather modest 0.09. In Figure 11 we show the fitted models overlayed on the spectra for stars in NGC 1770. Most of the stars—L17, L22, L25, L26, and L34—were extremely well fitted by a small range of Kurucz model atmospheres. The fits for L2 and L3 were acceptable, but less satisfactory. The fits for NGC 1770 suggest that the reddening in this cluster is more varied than that found in NGC 2014, ranging from 0.09 to 0.24.

We derived a stellar radius from the angular diameter using the relation $R_* = \theta^2 \times D$, where D is the distance to the LMC (50 kpc). With this derived stellar radius and the effective temperature specified by the best-fitting Kurucz model, we derived the stellar luminosity and the bolometric magnitude, $M_{\rm bol}$, for each star. These are listed in Table 6. The resulting HRDs for each cluster are shown in Figures 12 and 13. As is implied by the fits presented in Figures 10 and 11, there are typically several combinations of stellar effective temperature, reddening, and log g that are good fits to the observed spectra. To reflect this range, we have plotted the mean values of $T_{\rm eff}$ and $M_{\rm bol}$. The error bars associated with each point represent the 1 σ deviation from those mean values. Those stars with well classified spectral types are distinguishable as the points with small error bars.

The evolutionary tracks are taken from the work of Schaerer et al. (1993) and are appropriate for a low-metallicity environment such as the LMC. The individual points along each evolutionary track correspond to particular ages as follows: open squares (1–2 Myr), filled squares (2–3 Myr), open triangles (3–4 Myr), filled triangles (4–5 Myr), open circles (5–6 Myr), filled circles (6–7 Myr), crosses (7–8 Myr), asterisks (8–9 Myr), and weyes (9–10 Myr). Stellar evolutionary tracks are heavily dependent upon the amount of mass loss the star undergoes during its lifetime. As we discuss in more detail in § 6, stellar mass-loss rates derived for O stars in the LMC are higher than what one would expect based on their stellar wind velocities. Given this, while the metallicities of the Schaerer et al. (1993) evolutionary tracks are appropriate for this study, it is not entirely clear that their mass-loss rates are. Schaller et al. (1992) have compared the resulting HRDs for two sets of models, where one model uses a mass-loss rate twice that of the other. Based on that comparison, it appears that unless the mass-loss rates for the stars in this study are more than twice that used by Schaerer et al. (1993), our main conclusions will not be greatly affected. The uncertainty in the mass-loss rates contribute an

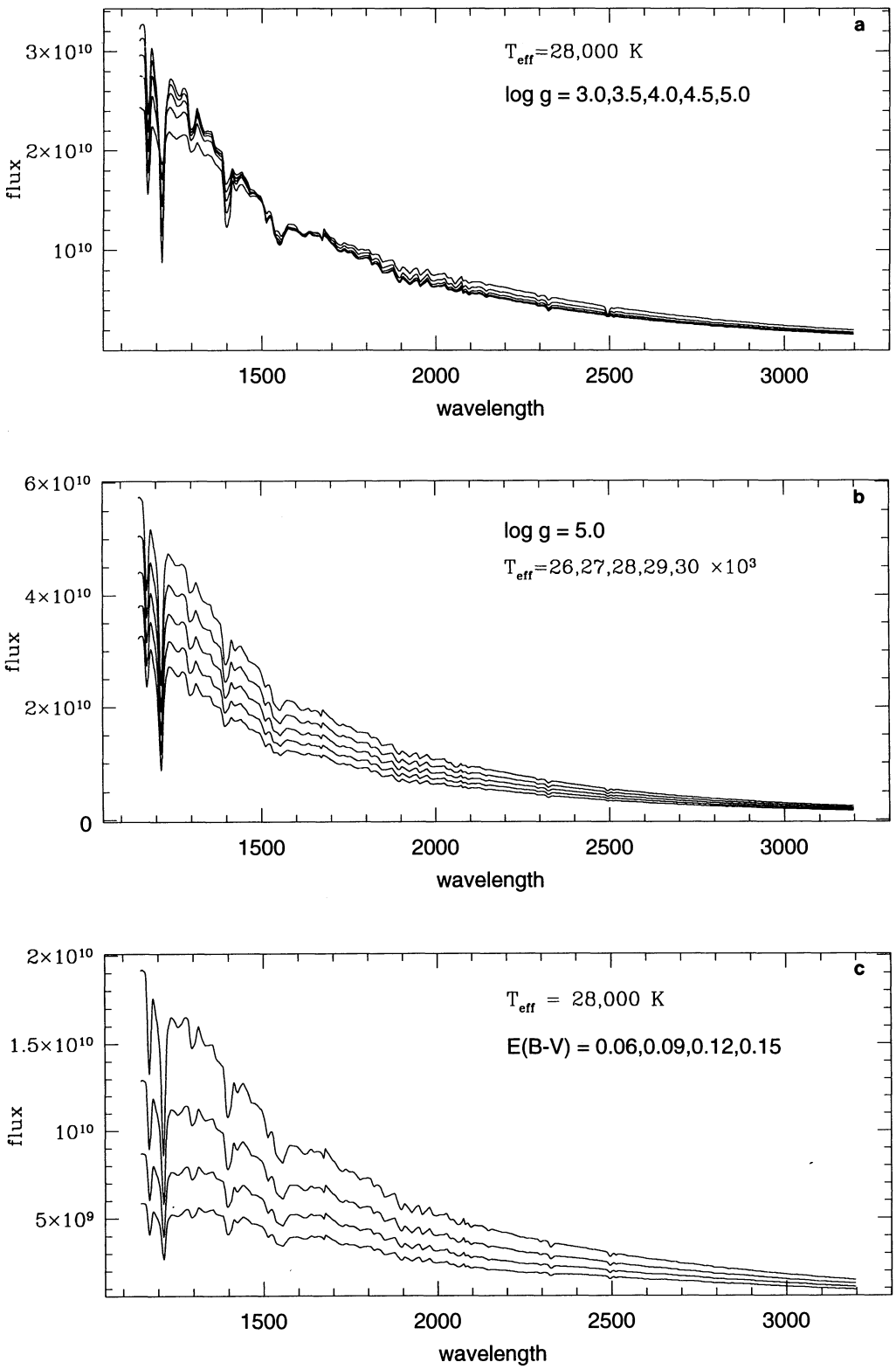

FIG. 9.—Effects of changing model parameters. (*a*) The differences between model spectra with a fixed effective temperature (28000 K), but with gravities ranging from 3.0 to 5.0 in steps of 0.5. (*b*) Spectra for models with fixed log g 5.0, but with temperatures ranging from 26000 to 30000 in steps of 1000 K. (*c*) A single model ($T_{\rm eff}$ = 28000, log g = 5.0) is shown reddened, using $E(B-V)$ values of 0.06, 0.09, 0.12, and 0.15.

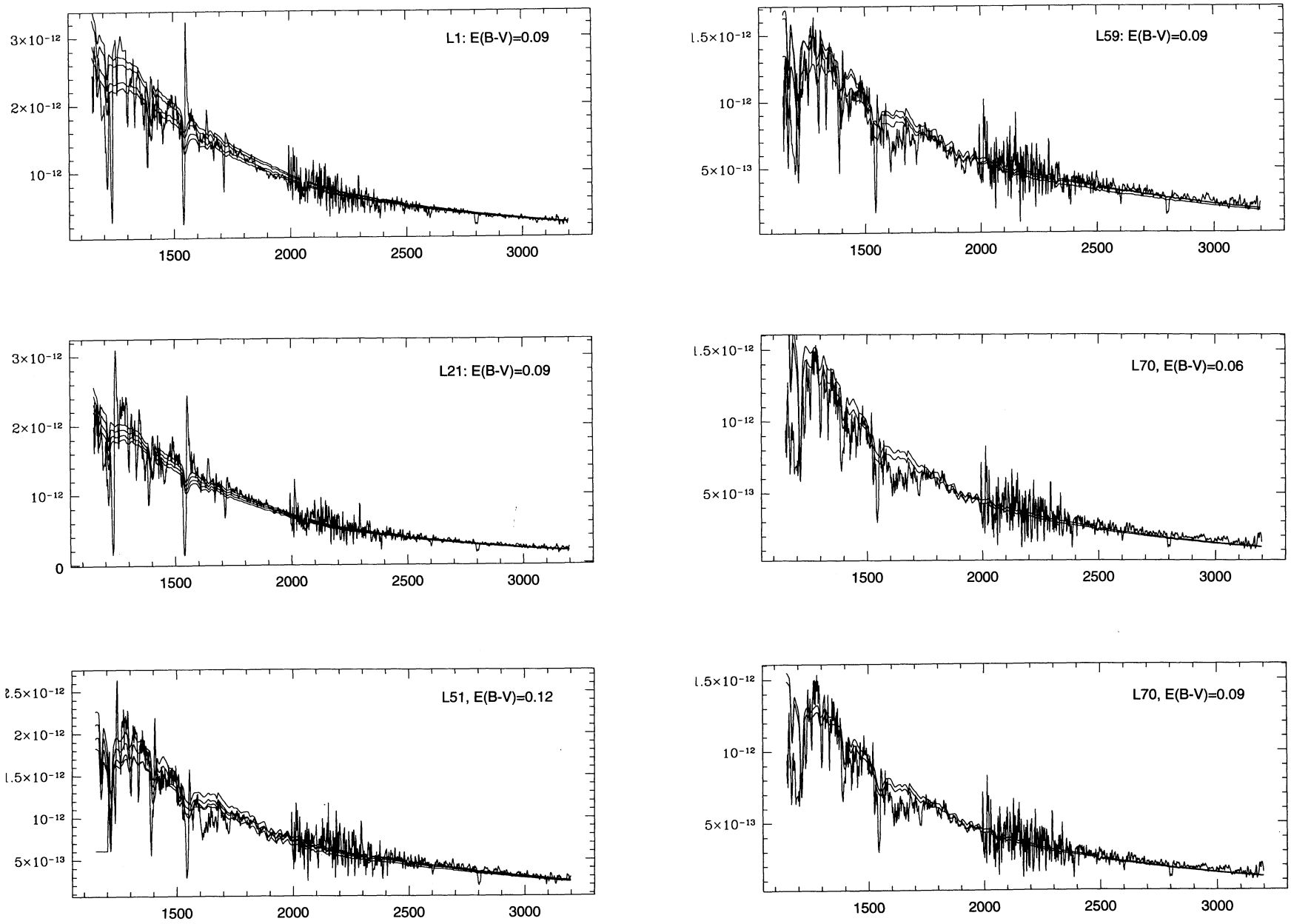

FIG. 10.—Observed spectra for each star in NGC 2014 overlayed with the curves of the best-fitting Kurucz atmosphere. Parameters of each fitted model are listed in Table 5a, b. The derived $E(B-V)$ value for each star is given in the upper right-hand corner.

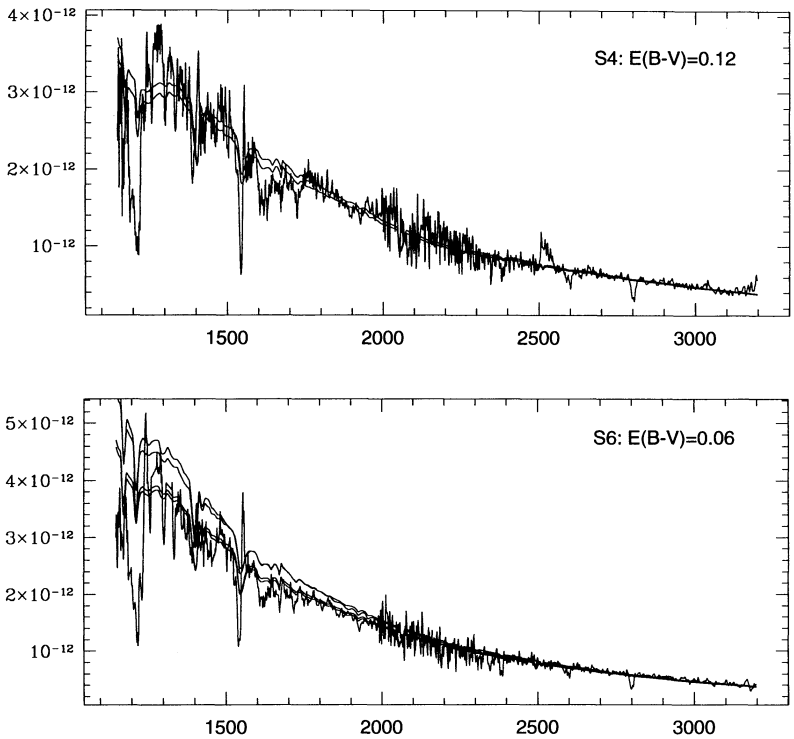

FIG. 10—*Continued*

uncertainty of 1–2 × 10^6 yr to the evolutionary tracks used in Figures 12 and 13.

4.1. *Implications of the H-R Diagrams*

From the HRD shown in Figure 12 it is evident that the most massive stars in NGC 2014—L1, L21, S4, and S6—all appear to have ages in the range of 2–4 × 10^6 yr. The other three stars studied here—L51, L59, and L70—are somewhat, older, having ages closer to 5–6 Myr. Although they do not determine an age for the cluster, Degioia-Eastwood et al. (1993) used optical photometry to determine that star formation in NGC 2014 appears to be coeval. Their analysis, however, did not include L1 or L21. Our results are consistent with this conclusion: the most massive stars in NGC 2014 appear to have formed within 2–4 Myr of each other. As discussed by Massey, Johnson, & Degioia-Eastwood (1995b), given the uncertainties inherent in this process, such a derived age spread should be considered essentially coeval. Additionally, we confirm that this is a relatively young cluster, having an age of only a few million years.

The HRD of NGC 1770 (Fig. 13) shows this cluster to be somewhat older than NGC 2014, with the most massive stars having ages of 5–6 Myr. There is, however, evidence of an older population of 15–20 $M_\odot$ stars with ages closer to 10 Myr. The full implications of this cannot be known without a derivation of the HRD for the intermediate mass stars, but an increasingly large number of OB associations in the Magellanic Clouds and the Galaxy are now known to contain a handful of older, 15–20 $M_\odot$ stars among a younger stellar population (e.g., Hillenbrand et al. 1993; Massey et al. 1995b). We should also note that our analysis does not include L43 (Sk-68 16), which has previously been classified as an O7 III star. We were also unable to obtain reliable spectra of several of the other bright stars in this cluster (e.g., L24 and L27). We conclude that these incomplete data suggest that star formation in NGC 1770 has not been coeval—that there is an age spread of at least 4–5 Myr. It remains to be seen whether the majority of the stars in the cluster were formed at the older or younger age.

4.2. *Spectral Types*

Given the derived effective temperatures listed in column (2) of Table 6, we are able to determine the approximate spectral types of the stars discussed here. Massey, Parker, & Garmany (1989), in calibrating optical photometric data, have derived a relationship between $T_{\rm eff}$ and the BC—BC = 23.5–5.9 log $T_{\rm eff}$. Making use of this relationship, we list the BC for each star in column (4). From the combination of $T_{\rm eff}$ and BC we used the calibrations of Garmany & Fitzpatrick (1988) and Humphreys & McElroy (1984) to determine the spectral types. These are listed in column (5) of Table 5. Not suprisingly, our results are quite consistent with those spectral types derived from optical spectroscopy. The one exception is L59, which we find to be two full spectral types earlier than its previously derived classification as a B2I star (Conti et al. 1986). As mentioned above, we had already found this star's UV spectrum to be entirely inconsistent with the published classification.

A secondary check on the accuracy of our derived spectral types was based on the examination of the spectra themselves. The spectra of OB stars are particularly useful in distinguishing between supergiants and main-sequence stars. Walborn & Panek (1984) found the Si IV resonance doublet at 1394, 1403 Å to be an excellent diagnostic of the luminosity class of O stars. In moving from main-sequence stars to supergiants, the Si IV doublet goes from being quite weak to displaying a full P Cygni profile. It is particularly strong in late-type O supergiants. Another broad diagnostic of O stars of all luminosity classes is the C IV line at 1548, 1551 Å (Walborn

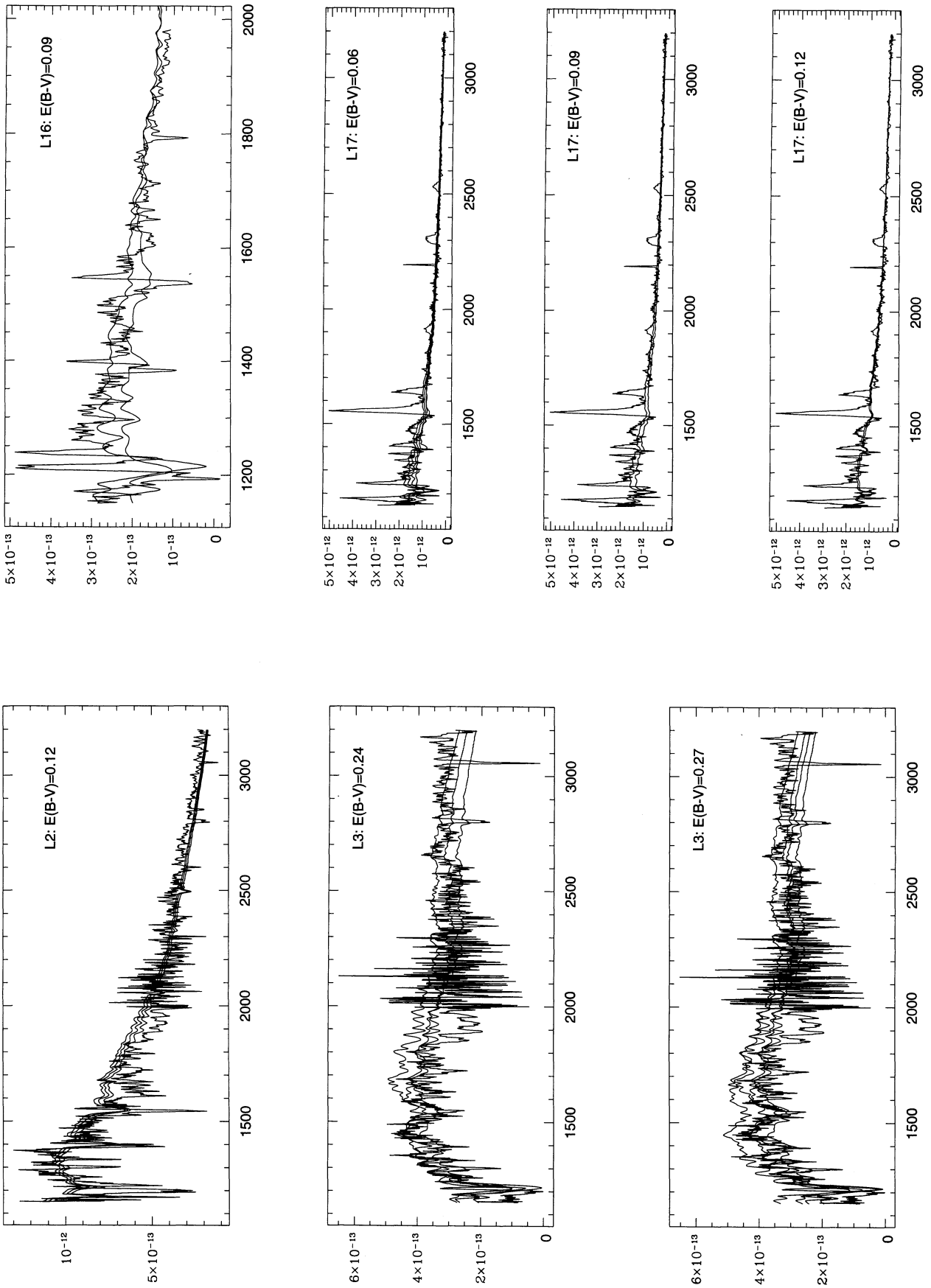

FIG. 11.—Same as Fig. 10, but for NGC 1770

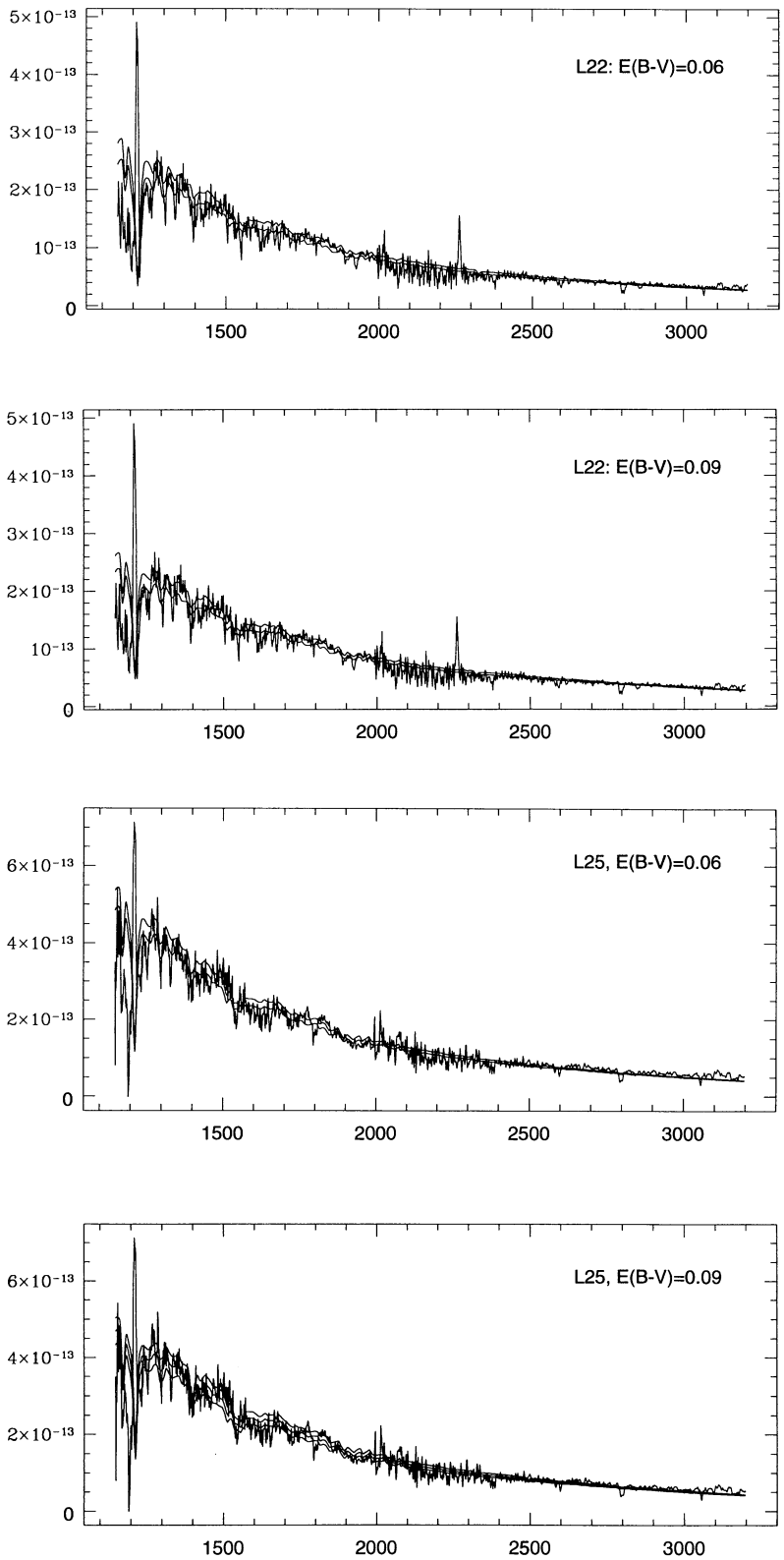

FIG. 11—*Continued*

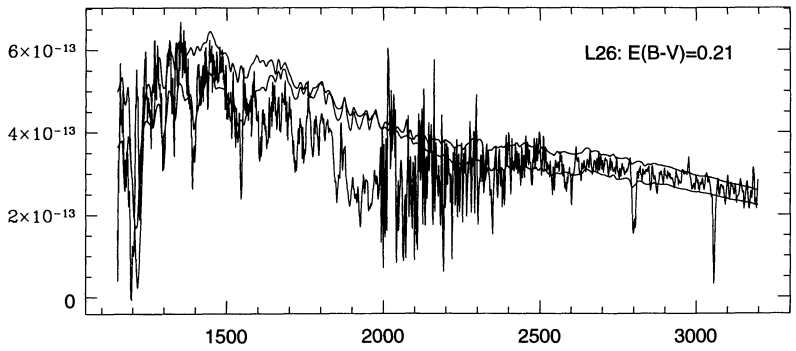

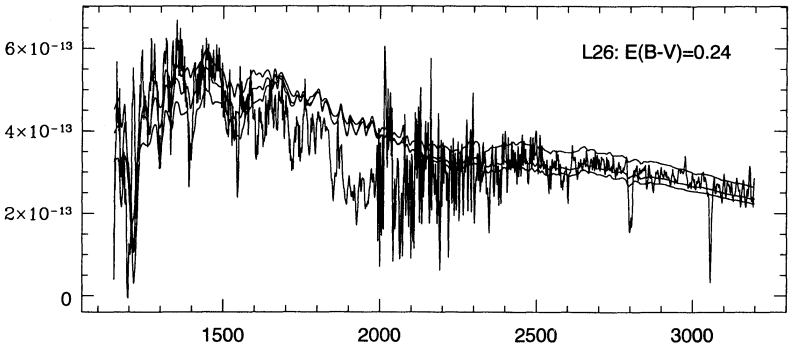

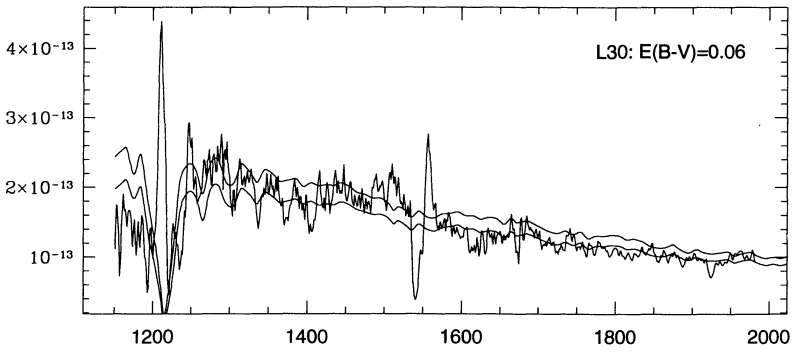

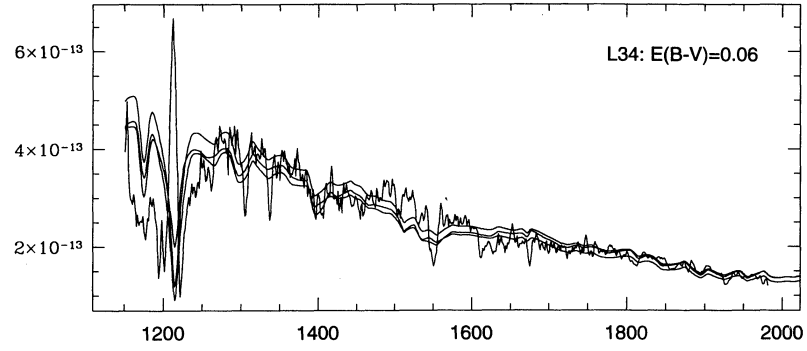

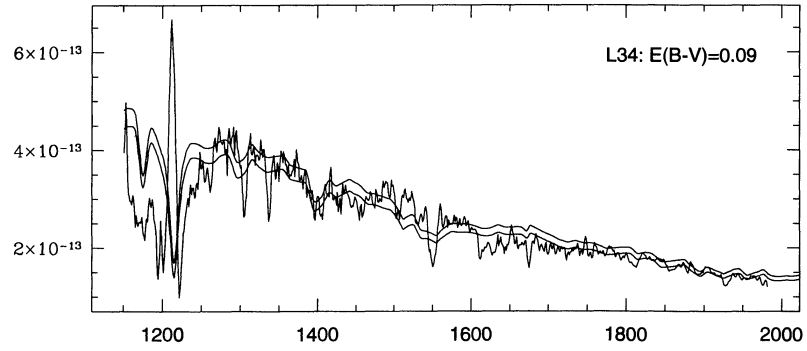

FIG. 11—*Continued*

TABLE 5

PARAMETERS FOR EACH MODEL

Star (1)	T_{eff} (2)	log g (3)	BC (4)	$E(B-V)$ (5)
NGC 1770: FITTED MODELS				
L2	29,000	3.50	−2.92	0.12
L2	30,000	3.50	−2.99	0.12
L2	31,000	3.50	−3.06	0.12
L3	16,000	2.50	−1.51	0.24
L3	16,000	5.00	−1.53	0.24
L3	17,000	2.50	−1.66	0.24
L3	17,000	2.50	−1.66	0.27
L3	17,000	5.00	−1.69	0.27
L3	18,000	2.50	−1.79	0.27
L3	18,000	5.00	−1.84	0.27
L16.....	19,000	2.50	−1.92	0.09
L16.....	19,000	5.00	−1.98	0.09
L17.....	23,000	5.00	−2.47	0.06
L17.....	24,000	3.00	−2.48	0.06
L17.....	24,000	5.00	−2.58	0.06
L17.....	25,000	5.00	−2.68	0.06
L17.....	26,000	5.00	−2.77	0.09
L17.....	27,000	5.00	−2.86	0.09
L17.....	30,000	5.00	−3.10	0.12
L17.....	31,000	5.00	−3.17	0.12
L22.....	22,000	5.00	−2.36	0.06
L22.....	23,000	5.00	−2.47	0.06
L22.....	24,000	4.00	−2.55	0.09
L22.....	24,000	5.00	−2.58	0.09
L22.....	25,000	5.00	−2.68	0.09
L25.....	25,000	5.00	−2.68	0.06
L25.....	26,000	5.00	−2.77	0.06
L25.....	27,000	5.00	−2.86	0.09
L25.....	28,000	5.00	−2.95	0.09
L25.....	29,000	5.00	−3.03	0.09
L26.....	19,000	2.50	−1.92	0.24
L26.....	19,000	5.00	−1.98	0.24
L26.....	18,000	2.50	−1.79	0.21
L26.....	18,000	3.50	−1.82	0.21
L26.....	18,000	5.00	−1.84	0.21
L30.....	18,000	5.00	−1.84	0.06
L30.....	19,000	5.00	−1.98	0.06
L34.....	24,000	5.00	−2.58	0.06
L34.....	25,000	4.00	−2.64	0.06
L34.....	25,000	5.00	−2.68	0.06
L34.....	27,000	5.00	−2.86	0.09
L34.....	28,000	5.00	−2.95	0.09
NGC 2014: FITTED MODELS				
L1	37,500	4.50	−3.58	0.09
L1	40,000	4.50	−3.77	0.09
L1	42,500	5.00	−3.96	0.09
L1	45,000	5.00	−4.14	0.09
L21.....	375,00	5.00	−3.59	0.09
L21.....	40,000	5.00	−3.77	0.09
L21.....	42,500	5.00	−3.96	0.09
L21.....	45,000	5.00	−4.14	0.09
L51.....	27,000	5.00	−2.86	0.12
L51.....	28,000	4.00	−2.89	0.12
L51.....	28,000	5.00	−2.95	0.12
L51.....	29,000	5.00	−3.03	0.12
L59.....	25,000	3.50	−2.61	0.09
L59.....	25,000	5.00	−2.68	0.09
L59.....	26,000	4.00	−2.73	0.09
L70.....	28,000	5.00	−2.95	0.06
L70.....	29,000	5.00	−3.03	0.06
L70.....	31,000	5.00	−3.17	0.09
L70.....	32,000	5.00	−3.23	0.09
S4	37,500	4.50	−3.58	0.09
S4	40,000	4.50	−3.77	0.09
S6	34,000	4.00	−3.31	0.06
S6	35,000	4.00	−3.38	0.06
S6	35,000	5.00	−3.42	0.06
S6	37,500	4.50	−3.58	0.06

TABLE 6

RESULTS

Star (1)	log T_{eff} (2)	M_{bol} (3)	BC (4)	Spectral Type (5)
NGC 1770				
L2	4.48 ± 0.01	−9.33 ± 0.06	−2.93 ± 0.01	B0 III
L3	4.22 ± 0.02	−9.62 ± 0.16	−1.39 ± 0.02	B2 I
L16.....	4.28 ± 0.01	−7.42 ± 0.03	−1.75 ± 0.01	B1 I
L17.....	4.42 ± 0.04	−9.02 ± 0.26	−2.58 ± 0.04	B0 V
L22.....	4.37 ± 0.02	−6.88 ± 0.16	−2.28 ± 0.02	B1 III
L25.....	4.43 ± 0.02	−7.59 ± 0.16	−2.64 ± 0.02	B0 III
L30.....	4.26 ± 0.01	−6.68 ± 0.05	−1.63 ± 0.01	B2 III
L34.....	4.41 ± 0.02	−7.49 ± 0.18	−2.52 ± 0.02	B0.5 III
NGC 2014				
L1	4.60 ± 0.03	−10.18 ± 0.20	−3.64 ± 0.03	O4 I
L21.....	4.61 ± 0.03	−9.91 ± 0.19	−3.70 ± 0.03	O4 I
L51.....	4.45 ± 0.01	−9.77 ± 0.06	−2.76 ± 0.01	B0 I
L59.....	4.40 ± 0.01	−9.11 ± 0.04	−2.46 ± 0.01	B0 I
L70.....	4.48 ± 0.02	−8.85 ± 0.16	−2.93 ± 0.02	B0 III
S4	4.59 ± 0.02	−10.76 ± 0.09	−3.58 ± 0.02	O8 V
S6	4.55 ± 0.02	−10.16 ± 0.10	−3.35 ± 0.02	O8 I

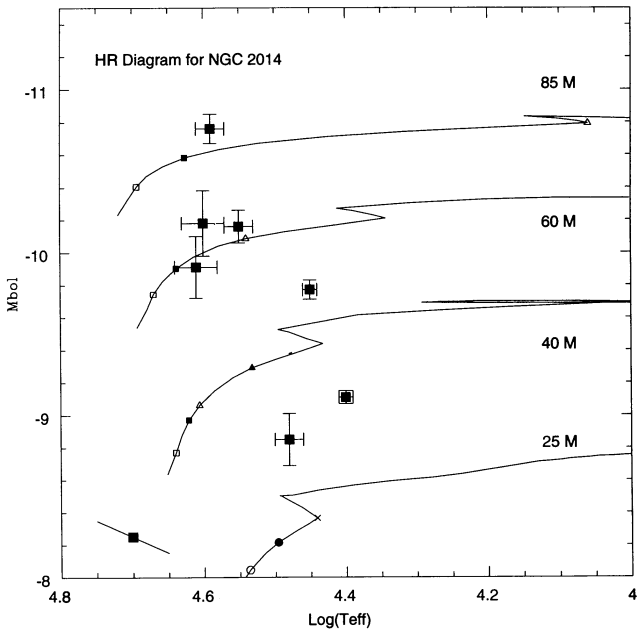

FIG. 12.—HRD for the targeted stars in NGC 2014. The points represent the mean of the fitted models for each star. Error bars correspond to the standard deviations of those means. In the lower-left-hand corner we have plotted the error bars corresponding to an uncertainty in the stellar $T_{\rm eff}$ of 3000 K. Derived parameters for each star are listed in Table 6. We have used the evolutionary tracks of Schaerer et al. (1993), and the individual points along each track correspond to particular ages as follows: 1–2 Myr (*open squares*), 2–3 Myr (*filled squares*), 3–4 Myr (*open triangles*), 4–5 Myr (*filled triangles*), 5–6 Myr (*open circles*), 6–7 Myr (*filled circles*), 7–8 Myr (*crosses*), 8–9 Myr (*asterisks*), and 9–10 Myr (*weyes*).

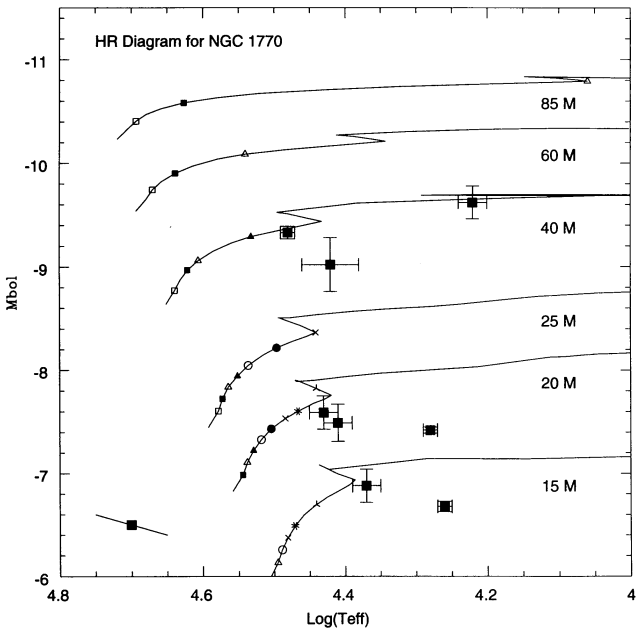

FIG. 13.—Same as Fig. 12, but for NGC 1770

& Panek 1984). This line, however, is not useful for distinguishing between O spectral types or luminosity classes, because it is typically seen as a P Cygni profile in all O type stars.

Using these criteria, we examined each of the observed spectra in order to determine their luminosity class and rough spectral type. Based on the presence of a strong P Cygni profile at the Si IV line, L51, L59, S4 (in NGC 2014), and L16 (in NGC 1770) are all supergiants. That L21 and L1 are also classified as supergiants but do not exhibit P Cygni profiles at Si IV is not surprising, since this correlation breaks down for the early O type stars (Walborn & Panek 1984). A borderline case is that of S6. It does not have a strong P Cygni profile at Si IV, although it does appear to have a strong Si IV absorption feature. It is, therefore, not likely to be a luminosity class I object, although the strength of the Si IV absorption is consistent with a classification as a luminosity class II or III star. This is consistent with previous spectral classifications, as well as our derived $T_{\rm eff}$ and BC. Those stars with strong P Cygni profiles at the C IV lines should be classified as O stars, and this is the case for the stars studied here.

5. STELLAR WINDS

It is well known that massive stars show a certain amount of mass loss associated with a strong stellar wind driven by momentum being transferred to the gas by absorption and scattering of line radiation (Castor, Abbot, & Klein 1975; Abbott 1982; Pauldrach, Puls, & Kudritzk; 1986). O stars lose a significant amount of mass over the course of their lifetimes, and their outflows are manifested in the UV resonance lines (Bernabeu, Magazza, & Stalio 1989). The strongest of these features is the P Cygni profile of the C IV line at 1548 Å. According to the radiation-driven wind theory, the resulting mass-loss rate is proportional to the metallicity (Abbott 1982), and one would therefore expect that the mass-loss rates from O and B stars in the Magellanic Clouds would be significantly lower than those in their Galactic counterparts. This, however, does not seem to be the case. Garmany & Conti (1985) and Garmany & Fitzpatrick (1988) have found that while the stellar wind velocities in O and B stars in the Clouds are lower than in the Galaxy, the mass-loss rates are comparable (but see Böhm-Vitense & Hodge 1984). Such results, although containing some inherent uncertainty, cast doubt upon the radiation-driven wind theory.

Full analyses of the UV stellar wind lines (e.g., C IV) involve detailed line fitting of the P Cygni profiles (Bernabeu et al. 1989; Garmany, Olson, & Conti 1981). As pointed out by Garmany & Conti (1985) and Garmany & Fitzpatrick (1988), it is extremely difficult to carry out detailed line fitting of the P Cygni profiles in low-resolution *IUE* data. In order to circumvent this problem, we have adapted the procedure detailed by Garmany & Fitzpatrick (1988) to derive mass-loss rates for the stars in this study. Their approach is based on the equations derived by Olson (1982), primarily

$$g(\text{C IV})\dot{M} = 2.0 \times 10^{-15} \frac{1}{A_{\rm c}} \frac{R_*}{R_\odot} \left(\frac{v_\infty}{1000}\right)^2 \times T_B(\text{C IV})(1+\gamma)0.5\,. \quad (1)$$

In equation (1) g(C IV) is the fraction of carbon that is triply ionized, $\dot{M}$ is the mass-loss rate, $A_{\rm C}$ is the number abundance of carbon relative to hydrogen, R_* and $R_\odot$ are the stellar and solar radii, respectively, T_B(C IV) is the optical depth of the C IV line, and γ is the exponent in the radial optical depth scaling law. As Garmany & Fitzpatrick (1988) emphasize, one cannot derive either γ or T_B from low-resolution *IUE* observations, and neither g(C IV) nor $A_{\rm C}$ are particularly well known. Their solution has been to derive empirically the optical depth from

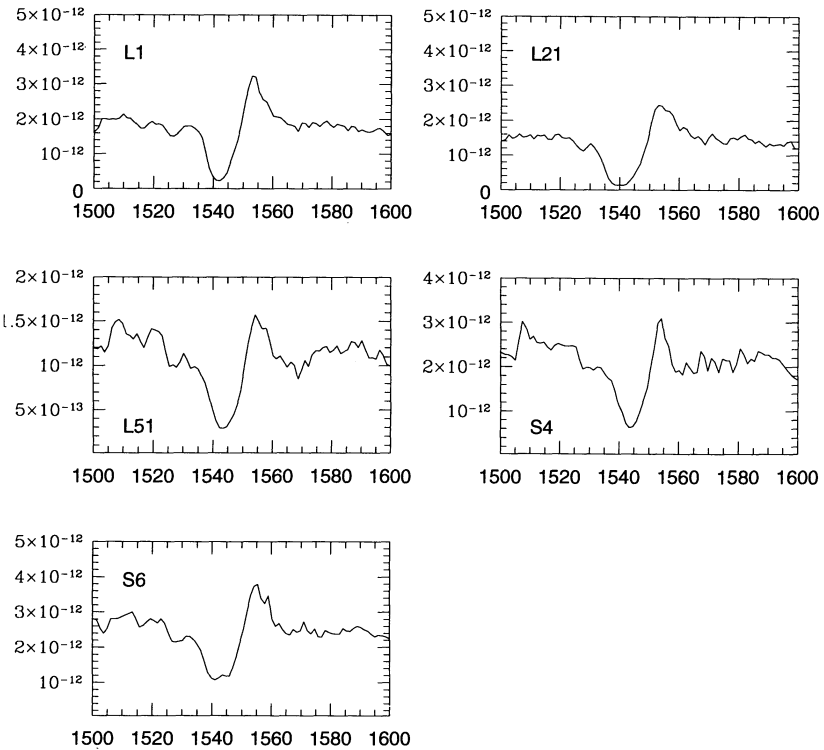

FIG. 14.—The C IV P Cygni profiles seen in the spectra of L1, L21, L51, S4, and S6. Note that the terminal wind velocities were measured using the point halfway between the C IV absorption and the blue continuum.

the equivalent width of the absorption component of the C IV P Cygni profile by comparing low-resolution spectra with high-resolution spectra, from which one can derive T_B. The resulting relationship is given in their equation (3). We also adopt their convention that γ is ~ 1.0, thus eliminating the last two terms in equation (1). As for the number abundance of carbon, we used the values derived by Russell & Bessell (1989) which show that A_C is 1.1×10^{-4}. Given these approximations, equation (1) reduces to two observed quantities: the equivalent width of the absorption component of the C IV P Cygni profile and the terminal velocity.

We measured V_∞ halfway between the minimum of the absorption component of the C IV P Cygni line and the blue edge of the continuum. The P Cygni profiles themselves are shown in Figures 14 and 15. The measured velocities were then corrected for the systemic velocity of the LMC, which was taken to be 270 km s^{-1} for NGC 1770 and 300 km s^{-1} for NGC 2014 (Rohlfs et al. 1984). Using these velocities, the measured equivalent widths of the absorption component (W_{abs}), and the stellar radii determined from the spectral fitting discussed in the previous sections, we derived the quantity g(C IV)$\dot{M}$ for each star. The results are listed in Table 7, where the first two columns are the stars' designation and their derived spectral type. The last four columns are the measured stellar wind velocity (V_∞), the equivalent width (EW), the calculated optical depth in the C IV line, and the mass-loss quantity (log $g\dot{M}$). We plot V_∞, W_{abs}, and log $g\dot{M}$ as functions of the

TABLE 7

STELLAR WIND PARAMETERS

Star (1)	Spectral Type (2)	V_∞ (3)	EW_{abs} (Å) (4)	T_B (5)	log $g\dot{M}$ (6)
		NGC 1770			
L16.....	B1 I	−2500 km s^{-1}	9.0	5.2	−8.3
L30.....	B2 III	−2300 km s^{-1}	8.8	4.9	−8.4
		NGC 2014			
L1	O4 I	−1800 km s^{-1}	8.2	4.1	−8.6
L21.....	O4 I	−2500 km s^{-1}	12.5	15.0	−7.9
L51.....	B0 I	−1800 km s^{-1}	8.8	4.9	−8.2
S4	O8 V	−1600 km s^{-1}	7.4	3.3	−8.7
S6	O8 I	−2000 km s^{-1}	7.9	3.8	−8.5

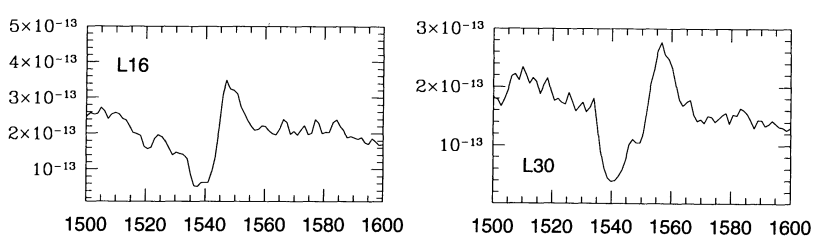

FIG. 15.—Same as Fig. 14, but for L16 and L30

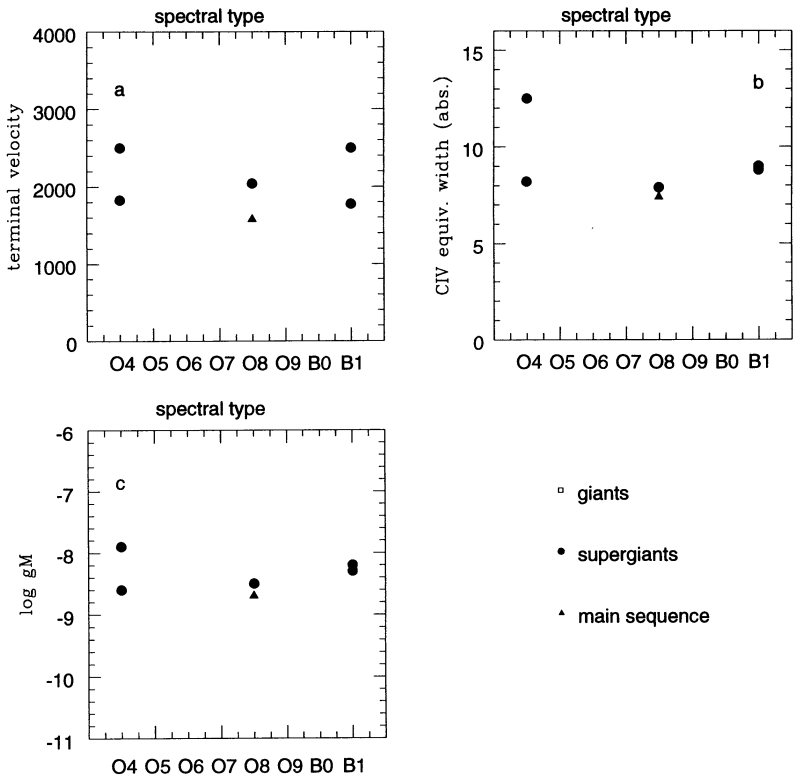

FIG. 16.—Stellar winds properties. The terminal velocities (measured halfway between the absorption minimum and the continuum) are shown in (*a*), the equivalent width of the C IV absorption component is shown in (*b*), and the derived equivalent mass-loss rates are shown in (*c*). The filled triangles are the luminosity class V objects, the open squares are the giants, and the filled circles are the supergiants.

spectral type in Figures 16*a* and 16*c*. What we find are the same general trends seen by Garmany & Conti (1985) and Garmany & Fitzpatrick (1988); the terminal wind velocities found in LMC stars tend to be somewhat smaller than those found in similar Galactic stars, at least for the O stars. We also see that the velocities found in this sample of stars are generally larger than those found in Small Magellanic Cloud (SMC) stars (Garmany & Fitzpatrick 1988). Similar trends are noted in the equivalent measurements as well. We do, however, find that the mass-loss rates (as expressed by log $g\dot{M}$) found here are comparable with those seen in Galactic and SMC stars (Garmany & Fitzpatrick 1988). This has been the general observation from several other studies of massive stars in the Magellanic Clouds; despite having smaller terminal wind velocities, O stars in the Clouds have mass-loss rates that are comparable to their Galactic counterparts. There are, of course, significant uncertainties associated with the method for determining the mass-loss rates employed here, and Garmany & Fitzpatrick (1988) discuss these in great detail.

6. SUMMARY

As part of a study of the ultraviolet properties of young clusters in the LMC, we have obtained *IUE* spectra of the massive stars in NGC 1770 and NGC 2014. Using a combination of these observed properties (both ultraviolet and optical) and stellar atmosphere models, we have derived the $T_{\rm eff}$, the log g, and the BC for each of the stars and plotted an HRD for each cluster. The results indicate that NGC 2014 is quite young ($\tau \sim 2$–5×10^6 yr) and that its star formation has been relatively coeval. This is consistent with the conclusions reached by Degioia-Eastwood et al. (1993). NGC 1770 is a bit older, and it has an apparent age spread of at least 4–5 $\times$ 10^6 yr, with the most massive stars ($\sim 40\ M_\odot$) being younger than the 15–20 $M_\odot$. Such trends have been noted in an increasingly large number of associations in the LMC and Galaxy (e.g., Hillenbrand et al. 1993, Massey et al. 1995b).

We have also used the *IUE* spectra of those stars with previously classified spectral types, to derive both an extinction curve and an estimate of the reddening toward each cluster. Only one star in NGC 1770 for which we had good UV information has been classified, and based on that star, we determined that the extinction curve closely matches that derived for stars in the 30 Dor complex (N81; F85). There are several stars in NGC 2014 that have been previously classified, and we found a similar trend for this cluster—the extinction curve is quite consistent with those of N81 and F85. In the case of NGC 2014, we derived a rather modest reddening value ($\sim$0.09) that is comparable with that derived by Degioia-Eastwood et al. (1993) for the cluster and by Caplan & Deharveng (1986) for the associated H II region. The reddening in NGC 1770 appears to be more varied, ranging from 0.09 to 0.24 within the cluster.

This study was made possible by NASA grant NAG 5-1444. We would like to thank the staff of the *IUE* Observatory for their help with the observations. We would also like to thank Lyla Taylor at GFSC for her help in the analysis of these data.

REFERENCES

Abbott, D. C. 1982, ApJ, 259, 282
Bernabeu, G., Magazza, A., & Stalio, R. 1989, A&A, 226, 215
Boggess, A., et al. 1978, Nature, 275, 372
Böhm-Vitense, E., & Hodge, P. 1984, in Structure and Evolution of the Magellanic Clouds, ed. S. van den Bergh & K. S. De Boer (Dordrecht: Reidel), 59
Calzetti, D., Kinney, A. L., & Storchi-Bergmann, T. 1994, ApJ, 429, 582
Caplan, J., & Deharveng, L. 1986, A&A, 155, 297
Cassatella, A., Barbero, J., & Geyer, E. H. 1987, ApJS, 64, 83
Castor, J. I., Abbott, D. C., & Klein, R. K. 1975, ApJ, 195, 157
Clayton, G. C., & Martin, P. G. 1985, ApJ, 288, 558
Conti, P. S., Garmany, C. D., & Massey, P. 1986, AJ, 92, 48
Degioia-Eastwood, K., Meyers, R. P., & Jones, D. P. 1993, AJ, 106, 1005
Fitzpatrick, E. L. 1985, ApJ, 299, 219 (F85)
———. 1986, AJ, 92, 1068 (F86)
———. 1988, ApJ, 335, 703
Fitzpatrick, E. L., & Garmany, C. D. 1990, ApJ, 363, 119
Garmany, C. D., & Conti, P. S. 1985, ApJ, 293, 407
Garmany, C. D., & Fitzpatrick, E. L. 1988, ApJ, 332, 711
Garmany, C. D., Olson, G. L., & Conti, P. S. 1981, 250, 660
Hillenbrand, L. A., Massey, P., Strom, S. E., & Merrill, K. M. 1993, AJ, 106, 1906
Hodge, P., Pastwick, L., Wilcots, E. M., & Olsen, K. 1996, in preparation
Humphreys, R. M., & McElroy, D. B. 1984, ApJ, 284, 565
Kennicutt, R. C., & Hodge, P. W. 1986, ApJ, 306, 130
Kurucz, R. L. 1979, ApJS, 40, 1
Lucke, P. 1972, Ph.D. thesis, Univ. Washington
Massey, P., Garmany, C. D., Silkey, M., & Degioia-Eastwood, K. 1989, AJ, 97, 107
Massey, P., Johnson, K. E., & Degioia-Eastwood, K. 1995b, ApJ, 454, 151
Massey, P., Lang, C. C., Degioia-Eastwood, K., & Garmany, C. D. 1995a, ApJ, 438, 188
Massey, P., Parker, J. W., & Garmany, C. D. 1989, AJ, 98, 1305
Murray-Hanson, M., & Clayton, G. 1993, AJ, 106, 1947
McNamara, D. H., & Feltz, K. A. 1980, PASP, 92, 587
Nandy, K., Morgan, D. H., Willis, A. J., Wilson, R., & Gondhalekar, P. M. 1981, MNRAS, 196, 955 (N81)
Olson, G. L. 1982, ApJ, 255, 267
Parker, J. W. 1993, AJ, 106, 560
Pauldrach, A., Puls, J., & Kudritzki, R. P. 1986, A&A, 164, 86
Rohlfs, K., Kreifschmann, J., Siegman, B. C., & Feitzinger, J. V. 1984, A&A, 137, 343
Russell, S. C., & Bessell, M. S. 1989, ApJS, 70, 865
Sanduleak, N. 1969, CTIO Contribution #89
Schaerer, D., Meynet, G., Maeder, A., & Schaller, G. 1993, A&AS, 98, 523
Schaller, D., Schaerer, D., Meynet, A., & Maeder, A. 1992, A&AS, 96, 269
Seaton, M. J. 1979, MNRAS, 187, 73P
van den Bergh, S. 1991, in The Magellanic Cloud, ed. R. Haynes & D. Milne (Dordrecht: Kluwer) 161
Walborn, N. R., & Panek, R. J. 1984, ApJ, 280, L27
Wilcots, E. M. 1994, AJ, 107, 1338